Effect of Freestream Parameters on the Laminar Separation in Hypersonic Shock Wave Boundary Layer Interaction

Vikash Kumar[1], Nishant[2], Md. Asif Hussain[3], Paragmoni Kalita[4]

[1] *vikashkumartu@gmail.com,* [2] *nishant_csb11@agnee.tezu.ernet.in*
[3] *asif47_meb11@agnee.tezu.ernet.in,* [4] *paragmk@tezu.ernet.in*
Department of Mechanical Engineering
Tezpur University, Napaam, Tezpur
Assam-784028, India

Abstract: Two-dimensional hypersonic flow over a ramped passage is computed on a finite volume framework using an in-house solver. van Leer's Flux Vector Splitting (FVS) scheme is used to compute the inviscid fluxes. The gradients in the viscous flux terms are computed using the Green's theorem. The effects of freestream parameters on the interaction between the boundary layer and the ramp-induced shock are investigated. For a given Reynolds number, the effects of freestream pressure and temperature on the laminar boundary layer separation are studied. It is seen that increase in freestream pressure reduces the flow separation; however increase in freestream temperature shifts the separation point upstream and the reattachment point downstream. Additionally the effect of Mach number at a given Reynolds number and freestream temperature on the boundary layer separation is discussed.

Keywords: Hypersonic, shock, boundary layer, freestream.

1. Introduction

Viscous interactions are prominent features of hypersonic flows especially for thin shock layer problems [1]. At very high speeds, the viscous dissipation on a solid surface leads to substantially high temperature, leading to increased viscosity. Thus the boundary layer becomes thicker and displaces the outer inviscid flow, thereby creating a leading edge shock wave. This type of viscous interaction, also called pressure interaction, influences the pressure field around the solid surface. Apart from the leading edge shock, the boundary layer may also interact with external shocks as well as shocks generated at other locations of the surface. This type of viscous interaction, also known as shock wave-boundary layer interaction (SWBLI), influences the dynamics of hypersonic flights a great deal.

Many subsystems for high speed applications involve flow over a ramped surface. The ramp induces an oblique shock. This leads to a strong shock wave-boundary layer interaction in such hypersonic flow applications. Some examples of such flows are engine inlets, wing-body junctions, control surfaces etc. One of the adverse effects of SWBLI is boundary layer separation [4]. Boundary layer separation affects the lift and drag characteristic of the vehicle by creating separation and reattachment shocks, expansion waves and slip lines. Detailed description about the practical model of ramp-induced SWBLI is available in reference [12].

In case of hypersonic flow over a ramped surface, when the ramp angle is greater than the incipient separation angle suggested by Needham and Stollery [17], then flow separation may take place near the ramp under certain flow conditions. Knowledge of the effects of the freestream parameters such as pressure, temperature and Mach number on the length of the separation bubble is important from the design point of view for hypersonic vehicles. Apart from boundary layer separation, the SWBLI phenomenon also leads to enhanced heating load [9] or even a turbulent re-attachment [5]. Both internal as well as external aerodynamics gets affected by such interactions.

Holden [7, 8] performed theoretical and experimental studies to understand the effect of freestream Mach number, Reynolds number, wedge angle and leading edge bluntness on SWBLI phenomena. Rizzeta and Mach [18] computed the laminar hypersonic flowfield for ramp induced SWBLI using four different numerical algorithms. John et al. [12] presented a numerical study of the effects of freestream Mach number and stagnation temperature on the boundary layer separation and heat transfer. Kalita and Dass [13] studied the effect of numerical diffusion on the laminar separation bubble length for the SWBLI problem. However, an exhaustive study of the effect of freestream temperature, pressure and Mach number at given freestream Reynolds number is not readily available in literature.

This work carries out a numerical investigation of the influence of freestream parameters like pressure, temperature and Mach number on the laminar separation in SWBLI for hypersonic flow over a ramped surface for a given freestream stagnation temperature and Reynolds number. The work aims at providing a qualitative insight into the effect of the freestream parameters on the separation and reattachment tendency by *numerical* simulation of the

governing equations, followed by analysis of the results through linking with the flow physics.

The governing equations for the viscous fluid flow are the Navier-Stokes equations. In the cell-centred finite volume computation of the Navier-Stokes equations for high speed flow applications, the inviscid flux terms across the cell interfaces are numerically evaluated by either central or upwind schemes, similar to the Euler fluxes. van Leer's FVS [2], Liou and Steffen's AUSM [15], Steger and Warming's FVS [19] etc. are some of the popular upwind methods. MacCormack's scheme [16], Local Lax-Friedrichs (LLF) or Rusanv's scheme [14], Jameson et al.'s JST scheme [10] etc. are examples of central schemes.

Many methods exist for the computation of the gradients in the viscous flux terms [11]. To compute the gradients at the cell faces due to the elliptic nature of the viscous terms even central differencing also leads a stable and accurate computation of the gradients across the cell-faces. However, this method can be used only in case of regular orthogonal grids. In the present work, since the grids are non-orthogonal, hence these terms are computed by the Green's theorem [3].

This paper is organized in five sections. In section 2, the governing equations and the numerical schemes used in the computations are introduced. Section 3 presents the problem statement and the boundary conditions. The results of the computations are presented along-with an analysis of the observations in section 4. Concluding remarks are made in section 5.

2. The Governing Equations and the numerical schemes

The flow is governed by the Navier-Stokes equations. The flow is modelled as two-dimensional. The inviscid fluxes are computed by using the van Leer's FVS scheme, which splits the flux at the cell interface based upon the sign of the eigenvalues of the flux Jacobian matrices. The mathematical formulation of the scheme is shown in sub-section B. The gradients in the viscous flux terms are computed by using the Green's theorem which is briefly discussed in sub-section *C*.

(A)   The Navier-Stokes equations

For 2D flow, the Navier-Stokes Equations are [6]:

$$\frac{\partial \mathbf{U}}{\partial t} + \frac{\partial \mathbf{F}_I}{\partial x} + \frac{\partial \mathbf{G}_I}{\partial y} = \frac{\partial \mathbf{F}_v}{\partial x} + \frac{\partial \mathbf{G}_v}{\partial y} \quad (1)$$

In these equations, $\mathbf{U}$ is the vector of conserved variables, $\mathbf{F}_I$ and $\mathbf{G}_I$ are the inviscid or convective flux vectors, $\mathbf{F}_v$ and $\mathbf{G}_v$ are the viscous flux vectors, where,

$$\mathbf{U} = \begin{bmatrix} \rho \\ \rho u \\ \rho v \\ \rho e_m \end{bmatrix} \quad \mathbf{F}_I = \begin{bmatrix} \rho u \\ p + \rho u^2 \\ \rho uv \\ (p + \rho e_m) u \end{bmatrix} \quad \mathbf{G}_I = \begin{bmatrix} \rho v \\ \rho vu \\ p + \rho v^2 \\ (p + \rho e_m) v \end{bmatrix}$$

and $\mathbf{F}_v = \begin{bmatrix} 0 \\ \tau_{xx} \\ \tau_{xy} \\ u\tau_{xx} + v\tau_{xy} - q_x \end{bmatrix}$ $\mathbf{G}_v = \begin{bmatrix} 0 \\ \tau_{xy} \\ \tau_{yy} \\ u\tau_{xy} + v\tau_{yy} - q_y \end{bmatrix}$

such that, e_m is the total fluid energy per unit mass and rest of the symbols have their usual meanings. These equations are solved by time-marching to obtain the steady state solutions. The first order Euler explicit technique is used for the time-integration.

The stress-tensor can be written using the indicial notation due to Einstein as follows.

$$\tau_{ij} = \mu \left(\frac{\partial u_i}{\partial x_j} + \frac{\partial u_j}{\partial x_i} \right) + \delta_{ij} \lambda \frac{\partial u_j}{\partial x_j} \quad (2)$$

The 2nd co-efficient viscosity is given by Stokes hypothesis,

$$\lambda = -\frac{2}{3} \mu \quad (3)$$

The heat fluxes along the x- and y- directions are given by

$$q_x = -k \frac{\partial T}{\partial x}, \quad q_y = -k \frac{\partial T}{\partial y} \quad (4)$$

The dynamic coefficient of viscosity μ is calculated by using the Sutherland's law [1]:

$$\frac{\mu}{\mu_0} = \left(\frac{T}{T_0} \right)^{\frac{3}{2}} \left(\frac{T_0 + 110}{T + 110} \right) \quad (5)$$

where, μ_0 and T_0 are the reference viscosity and reference temperature respectively. The thermal conductivity k is obtained from μ and a constant value of the Prandtl number (Pr) = 0.71 using the relation,

$$\text{Pr} = \frac{\mu c_p}{k} \quad (6)$$

Finally, the equation of state is used for the mathematical closure of the system of equations given by,

$$p = \rho RT \quad (7)$$

(B) The van Leer's Flux Vector Splitting Scheme

van Leer split the flux vector into two parts based upon the split Mach Number as [2]:

$$\mathbf{Q}_\perp = \mathbf{Q}_{\perp L}^+ + \mathbf{Q}_{\perp R}^- \quad (8)$$

where $\mathbf{Q}_\perp$ is the flux normal to the cell face and subscripts L and R represent the cells on the upstream and downstream sides of the cell face respectively. The Mach No. at the cell interface was obtained as,

$$M_{1/2} = M_L^+ + M_R^-$$

$$\text{with } M^\pm = \begin{cases} \frac{1}{2} \left(M \pm |M| \right), & \text{for } |M| \geq 1 \\ \pm \frac{1}{4} (M \pm 1)^2, & \text{otherwise} \end{cases} \quad (9)$$

The split fluxes are obtained in the following way:

$$\mathbf{Q}_{\perp}^{\pm} = \pm \frac{\rho a}{4}(M \pm 1)^2 \begin{bmatrix} 1 \\ \dfrac{n_x(u_\perp \pm 2c)}{\gamma} + u \\ \dfrac{n_y(u_\perp \pm 2c)}{\gamma} + v \\ \dfrac{\{(\gamma-1)u_\perp \pm 2c\}^2}{2(\gamma^2-1)} + \dfrac{u^2+v^2-u_\perp^2}{2} \end{bmatrix} \quad (10)$$

otherwise $\mathbf{Q}_\perp^+ = \mathbf{Q}_\perp, \mathbf{Q}_\perp^- = 0$ for $M \geq 1$

and $\mathbf{Q}_\perp^+ = 0, \mathbf{Q}_\perp^- = \mathbf{Q}_\perp$ for $M \leq -1$

Here n_x and n_y are the components of the unit normal vector to the cell face along the x- and y-directions respectively, $u_\perp$ is the contravariant velocity and c is the acoustic speed.

(C) The Green's theorem for computing the gradients

With reference to Fig. 1, at first the gradients of any flow variable φ inside the left (L) and right (R) cells sharing the interface are computed by using the following equations [3].

$$\left(\frac{\partial \varphi}{\partial x}\right)_{L/R} = \left(\frac{1}{\Omega}\int_{\partial\Omega}\varphi \, dS_x'\right)_{L/R} \approx \left(\frac{1}{\Omega}\sum_{m=1}^{N_F}\varphi_m S_{x,m}'\right)_{L/R}$$

$$\left(\frac{\partial \varphi}{\partial y}\right)_{L/R} = \left(\frac{1}{\Omega}\int_{\partial\Omega}\varphi \, dS_y'\right)_{L/R} \approx \left(\frac{1}{\Omega}\sum_{m=1}^{N_F}\varphi_m S_{y,m}'\right)_{L/R} \quad (11)$$

$$\left(\vec{\nabla}\varphi\right)_{L/R} = \left(\hat{i}\frac{\partial \varphi}{\partial x} + \hat{j}\frac{\partial \varphi}{\partial y}\right)_{L/R}$$

where, Ω is the volume of the cell, N_F is the number of cell-faces, $S_{x,m}'$ and $S_{y,m}'$ are the x- and y-components of the mth cell-face respectively.
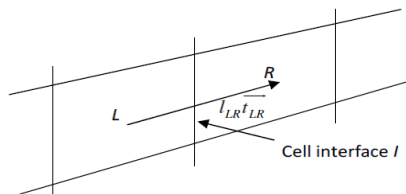
Figure 1: Two typical finite volume cells for computing the gradients across the in cell face

A provisional gradient at the midpoint of the cell interface I is obtained by averaging the gradients inside each adjoining control volumes L and R. The gradients within L and R are computed by using the Green's theorem given by equation (11).

$$\left(\overline{\nabla}\varphi\right)_{prov} = \frac{1}{2}\left[\left(\vec{\nabla}\varphi\right)_L + \left(\vec{\nabla}\varphi\right)_R\right] \quad (12)$$

Now the directional derivative along the connection between the cell-centroids is computed as,

$$\left(\frac{\partial \varphi}{\partial l}\right)_{LR} \approx \frac{\varphi_R - \varphi_L}{l_{LR}} \quad (13)$$

Such that l_{LR} represents the distance between the cell-centroids L and R. If $\vec{t}_{LR}$ is the unit vector connecting L and R, then

$$\vec{t}_{LR} = \frac{\vec{r}_{LR}}{l_{LR}} \quad (14)$$

where, $\vec{r}_{LR} = \vec{r}_R - \vec{r}_L$, so that $\vec{r}$ represents the position vector of a point. Finally the gradient at the cell interface is given by

$$\left(\vec{\nabla}\varphi\right)_I = \left(\overline{\nabla}\varphi\right)_{prov} - \left[\left(\overline{\nabla}\varphi\right)_{prov}.\vec{t}_{LR} - \left(\frac{\partial \varphi}{\partial l}\right)_{LR}\right]\vec{t}_{LR} \quad (15)$$

3. The problem statement and the boundary conditions

Hypersonic flow of air over a ramped surface is considered. As shown in Fig. 2, a weak shock emanates from the sharp leading-edge. This is named as the leading-edge shock. Due to strong viscous effects prevailing in hypersonic flows a boundary layer develops over the solid surface. Due to the ramp an oblique shock is developed. In case of inviscid flow, the oblique shock would have emanated from the compression corner itself. However in viscous flows, the oblique shock is formed upstream of the compression corner owing to viscous interactions. This shock is also called separation shock. Due to adverse gradients generated across the separation shock, and a ramp angle greater than the incipient separation angle, the boundary layer separates at the foot of the separation shock. The boundary layer reattaches downstream of the compression corner. A re-attachment shock emanates from this location. This shock intersects with the separation shock further downstream. The length of the laminar separation bubble is used as a measure of the severity of the boundary layer separation.

The length of the flat surface from the ramp upto the compression corner is taken as 0.05 m. The total length of the ramped passage along the x-direction is 0.12 m. The ramp angle is 15^0. The parameter $\mathrm{Re}_\infty = \rho_\infty U_\infty / \mu_\infty$ is taken as 8×10^5 m^{-1}, where ρ_∞, U_∞ and μ_∞ refer to the freestream density, velocity and dynamic coefficient of viscosity respectively. The wall temperature is 300 K. The computations are done at varying freestream static pressure and temperature. From earlier reporting [13], the results are considered to be grid-independent for the 300x360 mesh. The boundary conditions for the problem have to be implemented in conjunction with a careful choice of the computational domain. At the inlet, the freestream stagnation temperature, freestream Mach number, the parameter Re_∞ and the v-velocity are specified. Since the freestream is parallel to the x-axis, so the v-velocity at inlet is set as zero. At the wall, the velocity components in the dummy cell adjacent to the solid surface are computed by using the no-slip boundary condition. The pressure in the dummy cell is set equal to the value at the interior cell adjacent to the solid wall. The temperature at the dummy cell is set equal to the specified wall temperature. The density at the dummy cell is

calculated from the values of pressure and temperature in that cell by using the equation of state. At the outlet, all the variables are extrapolated from within the computational domain. The height of the computational domain is taken as 0.06 m [12] so that no discontinuities cross that boundary. Thus the freestream parameters are set as the top boundary condition.
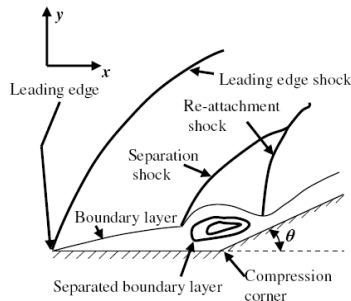
Figure 2: Schematic diagram representing 2D high speed flow over a compression corner involving SWBL interaction

4. Results and Discussion

The computations are done on a structured grid. A typical coarse grid is shown in Fig. 3. The effects of freestream pressure on the laminar separation for given freestream temperature and Reynolds number are studied. At $\mathrm{Re}_{\infty} = 8 \times 10^{5} \mathrm{~m}^{-1}$, the freestream temperature is kept constant at 120 K, 130 K, 140 K and 150 K. For every freestream temperature the freestream pressure is varied as 150 N/m², 200 N/m², 250 N/m², 300 N/m² and 350 N/m². Additionally, the effect of Mach number on the separation and re-attachment is investigated for the stagnation temperature of 1080 K and $\mathrm{Re}_{\infty} = 8 \times 10^{5} \mathrm{~m}^{-1}$ at Mach numbers 5, 6, 7 and 8.

The variations of the steady state skin friction coefficients along the ramped surface at freestream temperatures of 120 K and 150 K with varying freestream pressures are shown in Fig. 4 and 5 respectively. For clarity of the figures, only the plots corresponding to freestream pressures of 150 N/m², 250 N/m² and 350 N/m² are shown. It can be seen that in the attached region, the skin friction coefficient increases with increase in the freestream static pressure. This indicates that velocity gradient on the surface increases with freestream pressure, which will decrease the separation tendency.
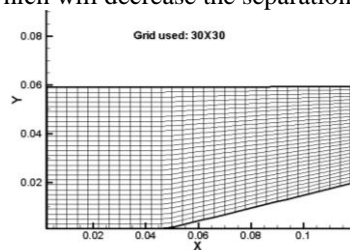
Figure 3: A typical coarse grid for the computation of the hypersonic SWBL interaction problem
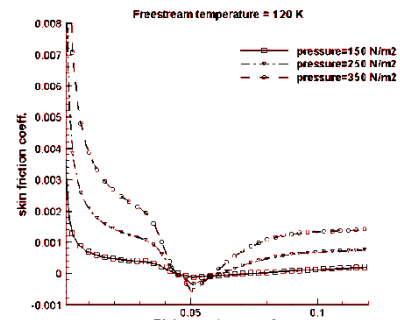
Figure 4: Skin friction coefficients along the surface at freestream temperature of 120 K and varying freestream pressures
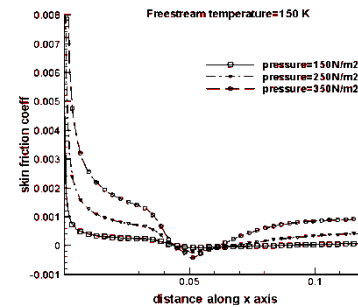
Figure 5: Skin friction coefficients along the surface at freestream temperature of 150 K and varying freestream pressures

Fig. 6 and 7 show the variations of the skin friction coefficients along the ramped surface at freestream pressures of 150 N/m² and 350 N/m² with varying freestream temperatures. For clarity the plots corresponding to freestream temperatures of 120 K and 150 K only are shown. Both the plots have the common trend that in the attached region, the skin friction coefficient increases with decrease in freestream temperature. This can be explained by the fact that higher freestream temperature increases the viscosity as per Sutherland's law, thereby increasing the boundary layer thickness. As the boundary layer thickens the velocity gradient at the solid surface decreases and hence the skin friction coefficient also decreases.
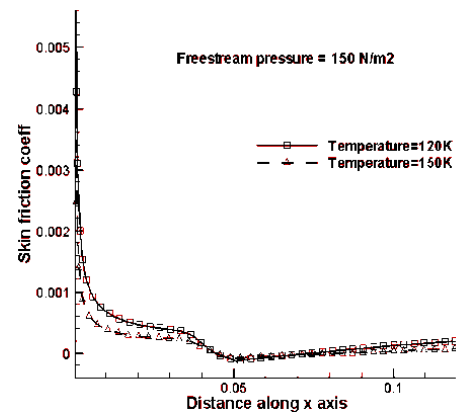
Figure 6: Skin friction coefficients along the surface at freestream pressure of 150 N/m² and varying freestream temperatures
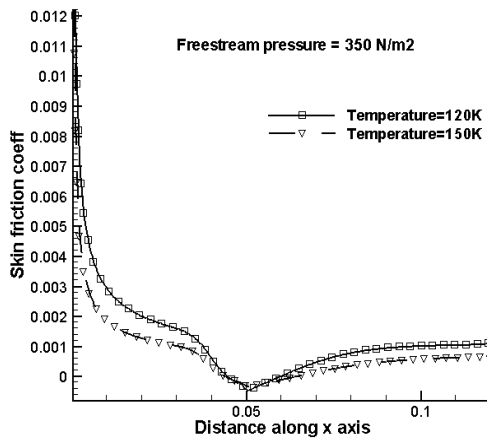
Figure 7: Skin friction coefficients along the surface at freestream pressure of 350 N/m^2 and varying freestream temperatures

The effects of freestream temperature and pressure on the separation bubble are studied from the point of view of points of separation and reattachment. Table 1 presents these locations as well as the laminar separation bubble (LSB) size at varying freestream pressures for given freestream temperatures of 120 K and 150 K. The effects of varying freestream temperatures for given freestream pressures of 150 N/m^2 and 350 N/m^2 on the separation and reattachment points along-with the LSB size are summarized in table 2.

Table 1 reveals that at a given freestream temperature, the location of the point of separation remains almost unaltered, but the point of reattachment advances with the increase in the freestream pressure, thereby decreasing the laminar bubble size. Thus it can be inferred that freestream pressure suppresses the laminar separation.

From Table 2, it can be observed that for given freestream pressure also, the location of the point of separation does not vary with the freestream temperature. But increase in the freestream temperature shifts the point of re-attachment further downstream, thus increasing the LSB size. This means that increase in freestream temperature raises the separation tendency. However at higher pressure, the LSB size is relatively less affected by temperature than at low pressure.

The variation of pressure coefficient along the *x*-direction for freestream temperature of 140 K and varying freestream pressures is shown in Fig. 8. For clarity, the plots for pressures of 150 N/m^2, 250 N/m^2 and 350 N/m^2 only are shown. The trend is similar at other freestream temperatures as well and so the plots at other freestream temperatures are not included here. The pressure coefficient is found to increase with increase in freestream pressure.

Fig. 9 shows the variation of pressure coefficient along the *x*-direction for freestream pressure of 250 N/m^2 and varying freestream temperatures. Here the plots only for temperatures 120 K and 240 K are shown. It is found that the pressure coefficient decreases with the increase in freestream temperature. The trend is found similar at other freestream pressures also are not shown in the present paper for paucity of space.

The variation of the skin friction coefficient along the surface at varying Mach numbers for freestream stagnation temperature of 1080 K and $\mathrm{Re}_\infty = 8 \times 10^5 \ \mathrm{m}^{-1}$ is shown in Fig.

10. In the attached region the skin friction coefficient decreases with the Mach number.

Table 1 Laminar separation and re-attachment vs freestream pressure for given freestream temperatures

Freestream temperature (K)	Freestream pressure (N/m^2)	Effect on LSB		
		Location of separation (mm)	Location of re-attachment (mm)	LSB size (mm)
120	150	44.2	73.4	29.2
	200	44.6	65.0	20.4
	250	44.6	61.4	16.8
	300	44.6	59.8	15.2
	350	44.6	59.0	14.4
150	150	44.6	84.2	39.6
	200	43.8	73.8	30.0
	250	43.8	67.4	23.6
	300	44.2	64.4	20.2
	350	44.2	63.8	19.6

Table 2 Laminar separation and re-attachment vs freestream temperature for give freestream pressures

Freestream pressure (N/m^2)	Freestream temperature (K)	Effect on LSB		
		Location of separation (mm)	Location of re-attachment (mm)	LSB size (mm)
150	120	44.2	73.4	29.2
	130	44.2	77.4	33.2
	140	44.2	81.0	36.8
	150	44.6	84.2	39.6
350	120	44.6	59.0	14.4
	130	44.6	60.6	16.0
	140	44.2	62.2	18.0
	150	44.2	63.8	19.6
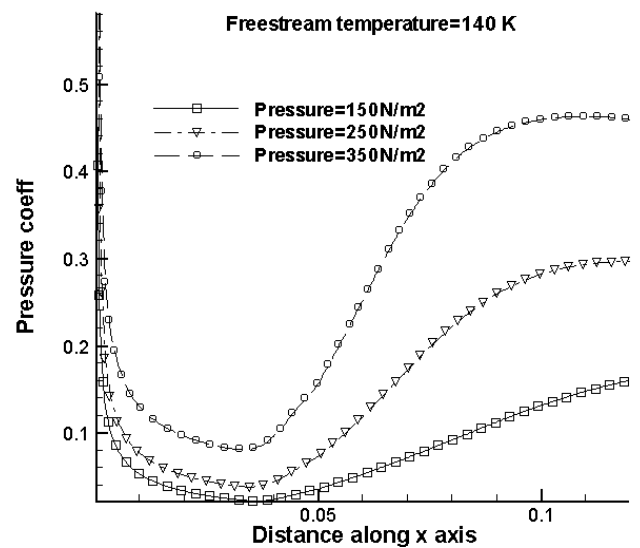
Figure 8: Pressure coefficients along the surface at freestream temperature of 140 K and varying freestream pressures
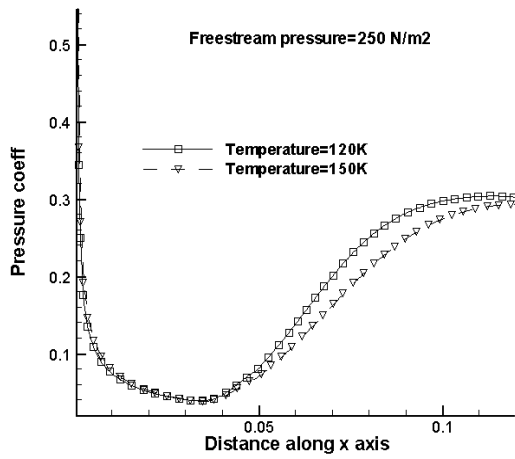
Figure 9: Pressure coefficients along the surface at freestream pressure of 250 N/m^2 and varying freestream temperatures

Table 3 shows the variation of the points of separation and reattachment and the LSB size with Mach number. It is evident that with increase in the Mach number the separation delays and the re-attachment advances, thus the LSB size decreases. In other words, the Mach number influences locations of both the separation as well as re-attachment points.

Table 3 Laminar separation and re-attachment vs Mach number

Mach number (M)	Effect on LSB		
	Location of separation (mm)	Location of re-attachment (mm)	LSB size (mm)
5	44.2	60.8	16.6
6	44.5	60.8	16.3
7	45.2	61.2	16.0
8	46.2	60.5	14.3
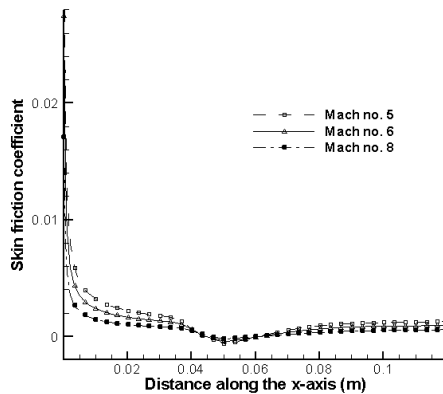
Figure 10: Skin friction coefficients along the surface at for fixed freestream stagnation temperature and Reynolds number

5. Concluding Remarks

Hypersonic shock-wave boundary layer interaction over a ramped surface is computed using the van Leer's FVS scheme. It is seen that the location of the point of separation does not change appreciably with freestream pressure and

temperature. However, the re-attachment point advances upstream when the freestream pressure is increased at a given freestream temperature. On the other hand, with the increase in freestream temperature at a given freestream pressure, the re-attachment point shifts further downstream, thereby increasing the separation length bubble size. In other words, increase in freestream pressure and decrease in freestream temperature lowers the separation tendency. The pressure coefficient increased with freestream pressure but decreases with freestream temperature. Mach number influences the locations of both separation and re-attachment points. Increase in Mach number delays the separation and advances the re-attachment.

References

[1] J. D. Anderson Jr., Hypersonic and High Temperature Gas Dynamics, McGraw Hill, pp. 13-24, 1989.

[2] W.K. Anderson, J.L. Thomas and B. van Leer, "Comparison of finite volume flux vector splitting for the Euler equations," AIAA J., vol. 24, No. 9, pp. 1435-1460, 1986.

[3] J. Blazek, Computational fluid dynamics: Principles and applications, Elsevier, pp. 267-293, 2001.

[4] D. R. Chapman, D. M. Kuehn and H.K. Larson, "Investigation of separated flows in supersonic and subsonic streams with emphasis on the effect of transition," NACA TN 3869, NACA Rep. 1356, 1957.

[5] M.C. Coet,, B. Chanetz and J.M. Delery, "Shock-Wave Boundary Layer Interaction with Entropy Layer Effect in Hypersonic Flow," ONERA, Colloque sur les Ecoulements Hypersoniques, Garchy, France, 1992.

[6] M. Delanaye, Polynomial reconstruction finite volume schemes for the compressible Euler and Navier-Stokes equations on unstructured adaptive grids, Ph. D. Thesis, University De Liege, pp. 15-19, 1996

[7] M.S. Holden, "Boundary-layer displacement and leading-edge bluntness effects on attached and separated laminar boundary layers in a compression corner. Part I: Theoretical study," AIAA J., vol. 8, pp. 2179–2188, 1970.

[8] M.S. Holden, "Boundary-layer displacement and leading-edge bluntness effects on attached and separated laminar boundary layers in a compression corner. Part II: Experimental study," AIAA J., Vol. 9, pp. 84–93. 1971.

[9] M.S. Holden and J.R. Moselle, "Theoretical and Experimental Studies of the Shock Wave-Boundary Layer Interaction on Compression Surfaces in Hypersonic Flow," ARL 70-0002, Aerospace Research Laboratories, Wright-Patterson AFB, OH, 1970.

[10] A. Jameson, "Analysis and design of numerical schemes for gas dynamics 1: Artificial diffusion, upwind biasing, limiters and their effect on accuracy and multigrid convergence," Int. J. Comput. Fl. Dyn., vol. 4, pp. 171–218, 1995.

[11] P. A. Jayantha and I.W. Turner, "A comparison of gradient approximations for use in finite volume models for two-dimensional diffusion equations," Num. Ht. Trnsf., Part B, vol. 40 pp. 367-390, 2001.

[12] B. John,, V. N. Kulkarni and G. Natrajan, "Shock wave boundary layer interactions in hypersonic flows," Int. J. Ht. Ms. Trnsf., vol. 70, pp. 81-90, 2014.

[13] P. Kalita, and A. K. Dass, "Effect of numerical diffusion on the computation of hypersonic shock wave boundary layer interaction," Proc. Int. Symp. Asp. Mech. Engg. Tech. Ind., NERIST, India, vol. 1, pp. 306-313, 2014.

[14] R. J. LeVeque, Finite volume methods for hyperbolic problems, Cambridge texts in Applied Mathematics, first edition, Cambridge University Press, pp. 232-234, 2002.

[15] M. S. Liou and C. J. Steffen, Jr., "A new flux splitting scheme," J. Comput. Phy., vol. 107, pp. 23-39, 1993.

[16] R. W. MacCormack, "The effect of viscosity in hypervelocity impact cratering," AIAAPaper, Cincinnati, Ohio, pp. 69-354, 1969.

[17] D.A. Needham, and J.L. Stollery, "Boundary-layer separation in hypersonic flow," AIAA paper, pp. 66-455, 1996.

[18] D. Rizzetta, and K. Mach, "Comparative numerical study of hypersonic compression ramp flows," AIAA Paper, pp. 89-1877, 1989.

[19] J. L. Steger and R.F. Warming, "Flux vector splitting of the inviscid gas dynamic equations with the application to finite difference methods," J. Comput. Phy., vol. 40, pp. 263-293, 1981.

Paragmoni Kalita, is working as an Assistant Professor in the Department of Mechanical Engineering, Tezpur University, India. He received his master degree in Heat Power Engineering form Banaras Hindu University, Varanasi (India) in 2004. He is also pursuing his Phd degree from Indian Institute of Technology, Guwahati, India.

Authors Profile

Vikash Kumar completed his B.Tech. degree in Mechanical Engineering from Department of Mechanical Engineering, Tezpur University in the year 2015.

Nishant completed his B.Tech. degree in Mechanical Engineering from Department of Mechanical Engineering, Tezpur University in the year 2015.

Md. Asif Hussain completed his B.Tech. degree in Mechanical Engineering from Department of Mechanical Engineering, Tezpur University in the year 2015.